Surface symmetry effect on the charge transfer at the black, blue, and green phosphorene/graphene interfaces

Zineb Kerrami, Yannick J. Dappe

Surface symmetry effect on the charge transfer at the black, blue, and green phosphorene/graphene interfaces

Zineb Kerrami[a,b,c], Salma Lahbabi[a,d], Yannick J. Dappe[b]
[a]Modeling, Simulation and Data Analysis (MSDA) Department, Mohammed VI Polytechnic University,
Benguerir 43150, Morocco
[b]SPEC, CEA, CNRS, Université Paris-Saclay, CEA Saclay, 91191 Gif-sur-Yvette Cedex, France
[c]LaMCScI, Faculty of Sciences B.P. 1014, Mohammed V University in Rabat, 10000 Rabat, Morocco
[d]EMAMI, LRI, ENSEM, University Hassan II Casablanca, Casablanca, Morocco

Abstract

In the present study, a comparative prediction of atomic and electronic structure of black, blue, and green phosphorene/graphene heterostructures is presented using Density Functional Theory (DFT). The lowest total and interaction energies and highest charge transfer correspond to the blue phosphorene/graphene interface, followed by black and green phosphorene/graphene interfaces. This trend is the same for monolayer, AA-, and AB-stacked bilayer graphene. However, the charge transfer is more important to AB-stacked bilayer grapheneat the interface with black and green phosphorene than to AA-stacked bilayer graphene. On another hand, for the charge transfer is more important from AA-stacked bilayer graphene to blue phosphorene, than from AB-stacked bilayer graphene. Besides, small bandgaps appear in phosphorene/bilayer graphene heterostructures, , resulting from the symmetry breaking due to the charge difference between the two layers of bilayer graphene. These findings provide useful insights on energetic stability of graphene/phosphorene heterostructures with promising properties for future nanoelectronics devices.

1. Introduction

Two-dimensional (2D) materials have become an exciting worldwide subject of research as they have triggered the apparition of new applications, mostly in nanoelectronics and energy conversion research field. There are numerous emerging 2D materials, each one with its own properties and applications [1−8]. For example, graphene, a semimetallic single layer of carbon atoms arranged in a 2D honeycomb lattice, has been intensively studied exploiting its unique mechanical and electronic properties. Hexagonal Boron nitride (hBN), which is made of an alternate arrangement of nitrogen and boron atoms, crystallizes in a similar structure as graphene but presents a large band gap of about 6 eV. It has been used as a potential protecting layer from contamination and oxidation for many 2D materials [9,10]. Besides the gapless graphene and the insulator hBN, transition metal dichalcogenides (TMDCs) provide promising alternatives as they exhibit diverse properties that depend on their composition, such as semiconductors (*e.g.*, MoS_2, $WS_{2, ...}$), superconductors (*e.g.*, $NbSe_2$, $TaS_{2, ...}$), semimetals (*e.g.*, WTe_2, $TiSe_{2, ...}$), and true metals (*e.g.*, NbS_2, $VSe_{2, ...}$) [11−13]. Semiconducting TMDCs have been successfully used for electronics [14,15], however they present some failures, notably, their smaller carriers mobilities compared to graphene, which limits their application in optoelectronic devices [16]. In this regard, light has been shed on black phosphorene (black phosphorus monolayer) as it preserves its direct bandgap in stacked forms with value that decreases gradually from 1.8 eV to 0.3 eV with the number of layers. In addition, its unique anisotropic structure due to armchair and zigzag edgesand its high carrier mobility up to 1000 $cm^2V^{-1}s^{-1}$ have already ensured novel uses for black phosphorene in optoelectronic and thermoelectric applications [17,18]. Recently, Zhu *et al*. [19] have predicted theoretically another phosphorene allotrope called blue phosphorene, which presents a very similar cohesion energy with respect to its black counterpart. Few years later, Zhang *et al*. [20] have synthesized a monolayer of blue phosphorene by epitaxial growth on an Au (111) substrate. Furthermore, Han *et al*. [21] reported a new allotrope of phosphorene called green phosphorene, which will be studied and compared to black and blue phosphorene in the following discussion. Geim *et al*. [22], suggested that 2D materials with such a wide variety of properties could be effectively used and combined to design and build vertical van der Waals (vdW) heterostructures with the exact desired characteristics. In that respect, each layer should see its properties preserved, providing potentially infinite possibilities for new electronics with better performance, and may lead to promising nano-electronic devices [23,24]. For instance, hexagonal Boron Nitride (hBN) has been coupled to graphene and phosphorene in vdW heterostructures to protect and preserve their electronic properties [10,25,26]. In addition, TMD/graphene heterostructures have been successfully used for transistors design [27−30]. Finally, C. Li et *al*. [31] have reported blue phosphorene/C_2N vdW heterostructure as an efficient model to enhance separation and migration of the photogenerated electrons and holes in C_2N and blue phosphorene, leading to an enhanced photocatalytic activity of the heterostructure.

In vdW heterostructures, surface symmetry plays a key role in the interactions at the interface. Controlling this feature might yield numerous interesting characteristics, which are still under discussion so far. In the present study, black, blue, and green phosphorene, each one with different atomic structure and surface symmetry, are combined with monolayer graphene, AA-bilayer graphene, and AB-bilayer graphene to construct vdW heterostructures. As a result, a

comparative study for the nine interfaces (phosphorene/Ggraphene) is presented, including stability and electronic properties of the three phosphorene allotropes. Then, the charge transfer at the interface between phosphorene allotropes and monolayer and bilayer graphene is discussed. Such comparison is of huge benefice to determine the energetic stability of phosphorene/graphene heterostructures and the mutual electronic exchange at the interface depending on phosphorene atomic structure.

2. Computational details

All calculations have been performed using the Quantum Espresso (QE) package [32] based on Density Functional Theory (DFT). Exchange and Correlation energies are described within the Perdew-Burke-Ernzerhof (PBE) functional under the Generalized Gradient Approximation (GGA) [33]. In order to accurately describe the interlayer weak van der Waals vdW interaction, the DFT-D2 method correction of Grimme has been adopted in all the calculations for graphene/phosphorene heterostructures [34]. The energy cutoff of the plane-wave basis set is set to 50 Ry, the convergences of the total energy difference between cycles and atomic forces acting on each atom for all the geometric structures are set to 10^{-6} eV and 0.01 eV/Å, respectively. Graphene/phosphorene heterostructures were built from the optimized monolayer and bilayer graphene and monolayer phosphorene unit cells as described in the following section (see Figure.2). To avoid interactions between periodic images along the z-axis, a 20 Å vacuum was added to the heterostructures. The reciprocal space is sampled within the Monkhorst-Pack scheme by $(12 \times 9 \times 1)$, $(12 \times 12 \times 1)$, and $(12 \times 4 \times 1)$ k-point grid for the black-phosphorene/graphene, blue-phosphorene/graphene, and green-phosphorene/graphene interfaces, respectively. The Heyd–Scuseria–Ernzerhof hybrid functional (HSE06) [35] method was used particularly to obtain accurate bandgap values of the black, blue, and green phosphorene as (HSE06) functional rectifies inaccurate PBE exchange functional by mixing this latter with a fraction of Hartree-Fock exact exchange [36]. The charge transfer analysis has been performed using Bader charge analysis [37].

3. Results and discussion

3.1 structural and electronic properties of black, blue, and green phosphorene

Side and top view of black, blue, and green phosphorene are presented in Figure 1, exhibiting significant structural differences. Black phosphorene presents a high anisotropy and structural differences that can be observed from a side view, such as armchair and zigzag edges. On another hand, blue phosphorene exhibits a structural pattern similar to graphene from a top view, and a flatter zigzag ridge than black phosphorene in both sides. Consequently, the layer thickness of blue phosphorene is reduced to 1.23 Å compared to 2.11 Å for black phosphorene. Green phosphorene contains three slightly buckled atomic layers instead of two as in the case of black and blue phosphorene. This leads to an increased phosphorene layer thickness (2.94 Å), which consists in zigzag ridges on one side and combined armchair and zigzag ridges on the other side (Fig.1(c)). As such, it has often been reported as a structural combination of black and blue phosphorene in previous reports [21].

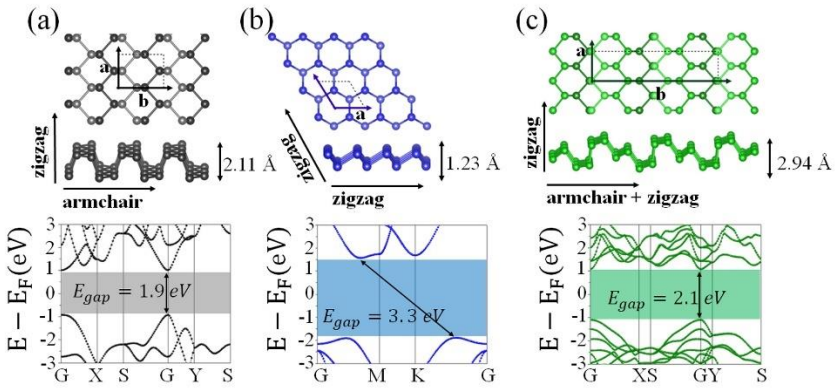

Figure 1 Top and side views of the atomic structure, and corresponding calculated band structures for (a) black, (b) blue, and (c) green phosphorene.

Calculated band structures for the different phosphorene allotropes presented in Figure 1 indicate that black phosphorene exhibits a direct bandgap of 1.9 eV, which is very interesting for optoelectronic applications [38,39]. Blue phosphorene presents an indirect bandgap of 3.3 eV that is large compared to the visible light energy, which limits its application in photonics. Green phosphorene presents an almost similar electronic behavior as black phosphorene, with a direct bandgap of 2.1 eV.

Table.1 Optimized lattice parameters a and b (Å) (note that a=b for blue phosphorene), corresponding calculated HSE06 band gap energy (eV), and total energy relative to black phosphorene energy per atom (meV/atom).

	a (Å)	b (Å)	Height (Å)	Band gap (eV)	Monolayer energy/atom (meV)
Black phosphorene	3.32	4.57	2.11	1.9	0
Blue phosphorene	3.30	3.30	1.23	3.3	36.61
Green phosphorene	3.31	14.14	2.94	2.1	11.92

The respective stability of the different phosphorene allotropes are summarized in Table.1. Total energies of green and blue phosphorene relative to black phosphorene are 11.92 meV/atom and 36.6 meV/atom respectively. However, that energy difference is considered small compared to the impact of external parameters such as substrate and temperature. Our calculated lattice parameters, electronic properties, and order of stability of black, blue, and green phosphorene are consistent with previous reports [21,40,41]. As the three phosphorene allotropes exhibit different structural and electronic properties, their interaction with graphene in an vdW heterostructure might present different behavior for each phosphorene allotrope. Thus, our objective is to provide insights in the effect of surface symmetry of phosphorene on its interaction with graphene.

3.2 Energy, stability, and electronic properties of phosphorene/monolayer graphene heterostructures

We now turn to the study of phosphorene/graphene interfaces. In order to simulate these heterostructures, two types of configurations for each phosphorene allotrope are considered. First we consider the interaction of one phosphorene layer on top of one graphene layer, and second on top of a graphene bilayer. This second configuration has been considered in the present study to take advantage from different electronic features that might arise from contact of phosphorene with a semimetallic (graphene) or potentially semiconductor (graphene bilayer) substrate. For all these configurations, a common set of lattice vectors has been considered. Hence, the supercell sizes have been chosen to limit, as much as possible, the mismatch strain between graphene and phosphorene lattice parameters, knowing that an exact matching would require a huge supercell, beyond our calculation possibilities. As illustrated in Figure 2 and Figure 7 (discussed in section 3.3 for phosphorene/bilayer graphene), black phosphorene/graphene heterostructures (BP/Gr and BP/2Gr) consist in a 3×2 black phosphorene supercell on top of a 4×2 rectangular graphene supercell. In the same manner, blue phosphorene/graphene heterostructures (blP/Gr and blP/2Gr) consist in a 3×3 blue phosphorene supercell on top of a 4×4 hexagonal graphene supercell. Finally, green phosphorene/graphene heterostructures (GP/Gr and GP/2Gr) consist in a 3×1 green phosphorene supercell on top of a 4×3 rectangular graphene.

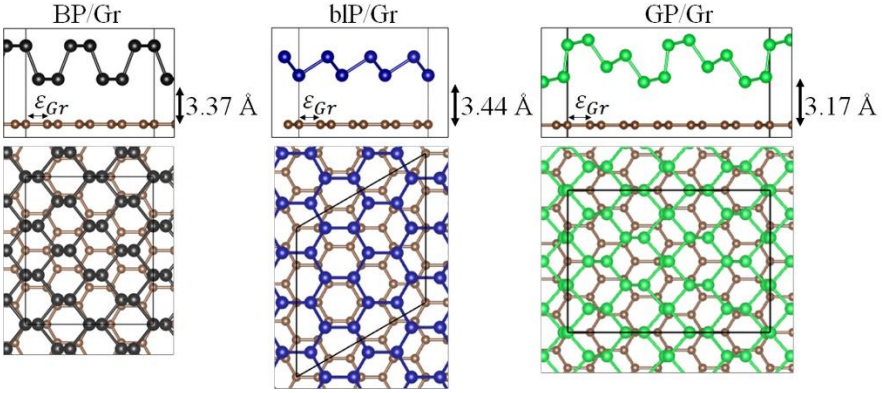

Figure 2 Top and side views of the atomic structures of black phosphorene/graphene (BP/Gr), blue phosphorene/graphene (blP/Gr), and green phosphorene/graphene (GP/Gr) heterostructures following phosphorene lattice vectors.

The interaction energy IE per unit atom that measures a configuration stability is defined by

$$\mathrm{IE} = ((E_{phosphorene/graphene} - (E_{phosphorene} + E_{graphene}))/N_P, \qquad (1)$$

where $E_{phosphorene/graphene}$, $E_{phosphorene}$, $E_{graphene}$ are the total energies of the phosphorene/grapheneinterface, phosphorene monolayer and graphene monolayer, respectively. N_P is the number of phosphorous atoms in the heterostructure. According to definition (1), a negative value of IE reflects an energetically favorable configuration. We note that for each phosphorene/graphene heterostructure, several stacking modes between phosphorene (black, blue, and green phosphorene) and graphene (monolayer graphene, AA-, and AB-bilayer graphene) have been tested and no energetically preferred stacking mode have

been found. This is consistent with weak van der Waals forces which are much less sensitive to local corrugation.

From a theoretical point of view, the application of strain on each monolayer in order to reach a common lattice parameter is an unavoidable restriction to simulate heterostructures. The ratio of applied strain varies depending on the studied systems [41]. For instance, in the present study, black phosphorene/graphene and green phosphorene/graphene heterostructures present a large strain along armchair ridges ($\geq$ 7%) and a small strain along zigzag ridges ($\sim$1%), while blue phosphorene/graphene heterostructures present a small strain ($\leq$0.7%). Therefore, as reported in previous studies [42], besides the mutual interaction between the constituents of the heterostructure, there is an effect of the applied strain on the electronic properties of each layer. However, phosphorene/graphene heterostructures present the same electronic behavior following both phosphorene and graphene lattice vectors. Thus, considering the flexibility of graphene under tensile strain, the phosphorene lattice vectors have been adopted to describe the electronic properties of phosphorene/graphene heterostructures.

The corresponding interlayer distances and interaction energies for phosphorene/graphene interfaces according to phosphorene and graphene lattice vectors are summarized in Table.2. As discussed in Section 3.1, phosphorous (P) atoms in the black, blue, and green phosphorene allotropes are not arranged as a single flat plane like in graphene, but belong to separate atomic planes along the z-axis. This implies a corrugated armchair/zigzag shape lateral configuration with different thicknesses. According to the presented results, two key comparisons can be performed. First, the heterostructures that follow graphene lattice vectors exhibit lower total energies and interaction energies compared to those that follow phosphorene lattice vectors. This could be related to the energetic response to applied strain, that is, according to the calculated total energies, higher under larger applied strain following phosphorene lattice vectors than that following graphene lattice vectors. Second, blue phosphorene/graphene heterostructures present the lowest total energies and interaction energies, and the largest interlayer distances, while green phosphorene/graphene heterostructures present the highest total energies and interaction energies, and consequently the shortest interlayer distances. The difference in interaction energy and interlayer distances trend can be explained by the difference in structural properties of phosphorene allotropes. Blue phosphorene/graphene heterostructure exhibits 9 atoms in the bottom plan (phosphorene plan in contact with graphene) and the lowest layer thickness. Black phosphorene/graphene exhibits 12 atoms and the higher layer thickness of black phosphorene. Green phosphorene/graphene exhibits 6 atoms and the highest layer thickness. Consequently, blue phosphorene/graphene heterostructure following graphene lattice vectors is the most stable configuration, while green phosphorene/graphene heterostructure following phosphorene lattice vectors is the less stable.

Table.2 Calculated strain percent ε(%) applied on graphene (phosphorene) following phosphorene (graphene) lattice vectors, interlayer distances (Å), total energy per number of phosphorous atoms (eV/P-atom) of phosphorene/graphene heterostructures, and interaction energies per number of phosphorous atoms (meV/P-atom) of phosphorene/graphene heterostructures.

	Lattice vectors	Strain ε (%)	Interlayer distance (Å)	Total energy (eV/P-atom)	Interaction Energy (meV/P-atom)
BP/Gr	BP	$\varepsilon(a_{Gr})$ = 1.05 $\varepsilon(b_{Gr})$ = 7.1	3.37	-416.59	-51.75
	Gr	$\varepsilon(a_{BP})$ = -1.04 $\varepsilon(b_{BP})$ = - 6.6	3.32	-416.76	-58.54
blP/Gr	blP	$\varepsilon(a_{Gr})$ = 0.70	3.44	-491.94	-58.89
	Gr	$\varepsilon(a_{blP})$ = -0.43	3.39	-491.94	-59.61
GP/Gr	GP	$\varepsilon(a_{Gr})$ = 0.86 $\varepsilon(b_{Gr})$ = 10.34	3.17	-416.42	-39.97
	Gr	$\varepsilon(a_{GP})$ = -0.85 $\varepsilon(b_{GP})$ = -9.37	3.08	-416.47	-43.24

We present in Figure 3 the bandstructure and projected density of states (PDOS) of black phosphorene/graphene heterostructures alongside the superposed bandstructures and density of states (DOS) of free-standing black phosphorene and graphene monolayers. For heterostructures (right panels), both black phosphorene direct band gap and Dirac cone of graphene have been preserved, which is characteristic of the weak van der Waals interaction. Though, the graphene Dirac cone shifts down below the Fermi level by 33.75 meV, corresponding to a small n-doping in graphene. This is representative of a small charge transfer from phosphorene to graphene as summarized in Table 3. These results are consistent with previously reported results [43].

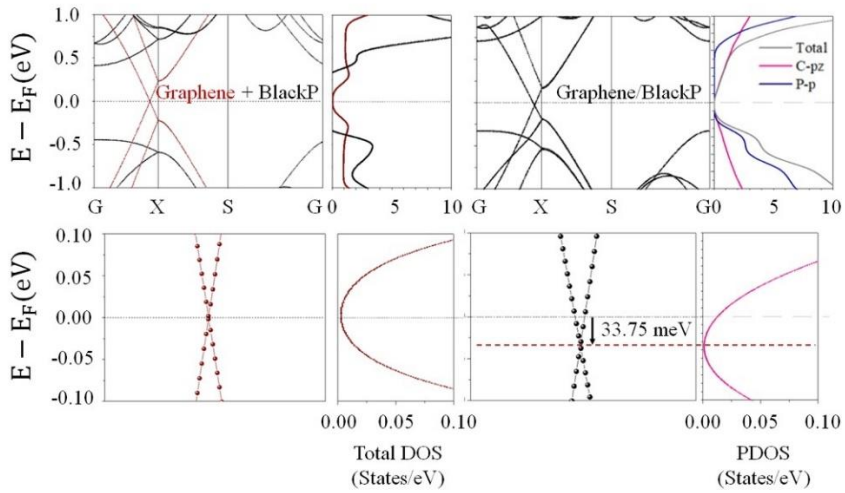

Figure 3 Calculated band structures and DOS of superposed free-standing black phosphorene and graphene (left), and black phosphorene/graphene (right) following black phosphorene lattice vectors. The bottom panels show the zoom-in band structure and DOS near the Dirac point. Black and red dashed lines present Fermi level and Dirac cone energy respectively.

Figure 4 presents the bandstructures of free-standing blue phosphorene and graphene monolayers, and blue phosphorene/graphene heterostructures. Contrarily to the black phosphorene/graphene heterostructure, the Dirac cone shifts up with respect to the Fermi level by 113.55 meV, corresponding to a p-doping in graphene.

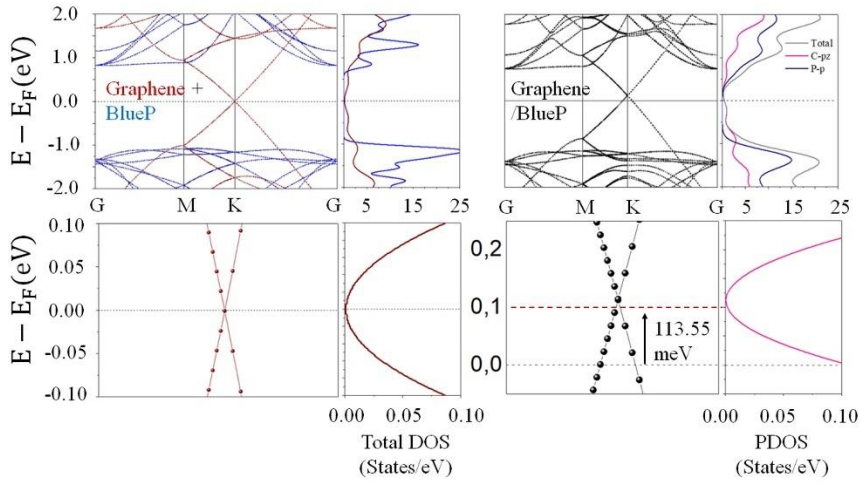

Figure 4 Calculated bandstructures and DOS of free-standing blue phosphorene and graphene (left), and blue phosphorene/graphene (right) following blue phosphorene lattice vectors. The bottom panels show the zoom-in band structure and DOS near the Dirac point. Black and red dashed lines present Fermi level and Dirac cone energy respectively.

Figure 5 presents the bandstructures of green phosphorene/graphene heterostructures. As for the previous heterostructures, both green phosphorene and graphene electronic behavior have been preserved. Namely, the bandgap energy of green phosphorene and the location of the graphene Dirac cone with respect to the Fermi level remain unchanged . This is due to the zero-charge transfer at the green phosphorene/graphene interface (see Table.3).

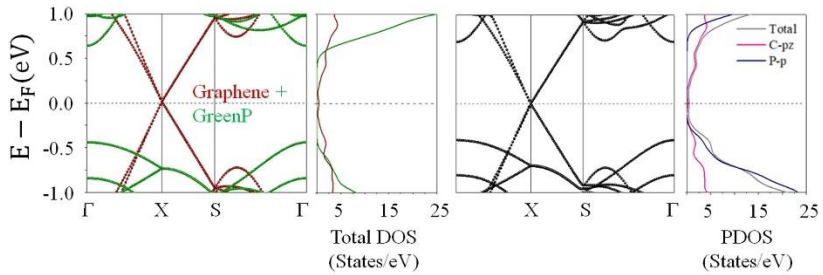

Figure 5 Calculated bandstructures and DOS of free-standing green phosphorene and graphene (left), and green phosphorene/graphene (right) following green phosphorene lattice vectors. Black dashed line presents Fermi level.

To get more insight on the interaction at the interface level, calculated difference in charge distribution ($\Delta\rho$) and planar averaged charge density along z-axis are presented in Figure 6(a). The charge distribution in black phosphorene/graphene heterostructure follows the structural corrugation of black phosphorene, leading to a charge accumulation (red) close to phosphorene, and depletion (cyan) close to graphene, around the armchair hollows of phosphorene and the opposite close to the bottom plan of phosphorene. For blue phosphorene/graphene heterostructure (Figure 6(b)), the charge distribution shows a net charge accumulation (red) close to blue phosphorene, and depletion (cyan) close to graphene. While for green phosphorene/graphene heterostructure the charge distribution reveals a poor charge density variation at the interface due to the lack of interaction.

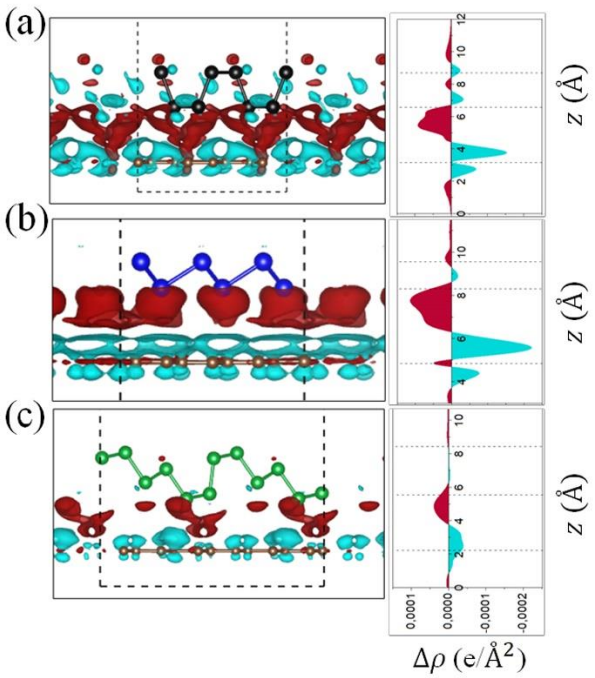

Figure 6 Difference in charge distribution and planar averaged charge density along z-axis in BP/Gr (a), blP/Gr (b), and BP/Gr (c) heterostructures. The cyan and red regions represent charge depletion and accumulation, respectively. The isosurface value is 0.0001 e/Å^3 and the horizontal dashed-dot lines denote the locations of atomic layers of graphene and phosphorene.

Table.3 Calculated Bader charge transfer for phosphorene/graphene heterostructures.

	Lattice vectors	Charge Transfer (e^-) (phosphorene to graphene)
BP/Gr	BP & Gr	+0.03
blP/Gr	blP & Gr	-0.04
GP/Gr	GP & Gr	~0.00

According to Bader charge analysis (see Table. 3), the estimated amount of charge transfer is around 0.04 electrons from graphene to blue phosphorene, which is a bit higher than what is calculated in the case of black phosphorene/graphene. This difference in charge transfer is consistent with the difference in Fermi level shift observed between black phosphorene/graphene and blue phosphorene/graphene.

In summary, no bandgap opening at the Dirac cone has been observed in all phosphorene/graphene heterostructures studied here, as expected from the weak van der Waals interactions. Blue phosphorene/graphene heterostructure presents the lowest interaction energy and highest charge transfer from graphene to blue phosphorene. It is followed by black phosphorene/graphene heterostructure that exhibits higher interaction energy, and lower charge transfer from black phosphorene to graphene, and then green phosphorene/graphene heterostructure that presents the highest interaction energy, and almost zero charge transfer.

3.3 Energy, stability, and electronic properties of phosphorene/bilayer graphene heterostructures

Figure 7 illustrates the atomic structures of black, blue, and green phosphorene/bilayer graphene heterostructures following phosphorene lattice vectors.

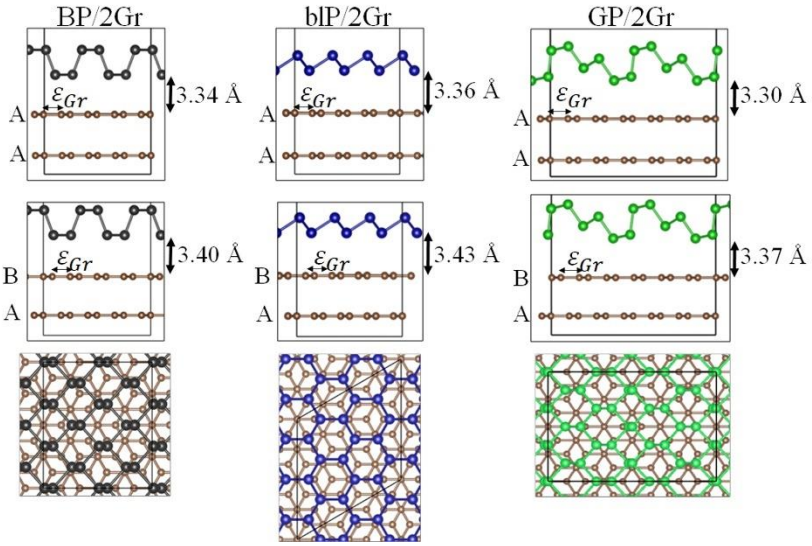

Figure 7 Top and side views of the atomic structures of black phosphorene/bilayer graphene (BP/2Gr), blue phosphorene/bilayer graphene (blP/2Gr), and green phosphorene/bilayer graphene (GP/2Gr) heterostructures following phosphorene lattice vectors.

The interlayer distances, total energies, and interaction energies for phosphorene/bilayer graphene heterostructures according to both (BP) and (Gr) lattice vectors are summarized in Table 4. Our first observation is that phosphorene/AB-graphene heterostructures exhibit lower interaction energies and shorter interlayer distances than phosphorene/AA-graphene heterostructures for the three phosphorene allotropes. This is related to the fact that bilayer graphene in AB stacking mode is energetically more stable than in AA staking mode [44]. Total and interaction energies for the three studied phosphorene allotropes follow the same trend as for phosphorene/monolayer graphene.

Table.4 Calculated strain ratio $\varepsilon(\%)$ applied on bilayer graphene (phosphorene) following phosphorene (graphene) lattice vectors, interlayer distances (Å), total energy per number of phosphor atoms (eV/P-atom) of phosphorene/bilayer graphene heterostructures, and interaction energies per number of phosphor atoms (meV/P-atom) of phosphorene/bilayer graphene heterostructures.

	Lattice vectors	Strain ε (%)	Interlayer distance (Å)	Total energy (eV/P-atom)	Interaction Energy (meV/P-atom)
BP/2Gr AA	BP	$\varepsilon(a_{Gr})$ = 0.98 $\varepsilon(b_{Gr})$ = 7.35	Gr-Gr = 3.47 BP-Gr = 3.34	-642.00	-105.46
	Gr	$\varepsilon(a_{BP})$ = -0.97 $\varepsilon(a_{BP})$ = -6.84	Gr-Gr = 3.43 BP-Gr = 3.31	-642.37	-118.21
BP/2Gr AB	BP	$\varepsilon(a_{Gr})$ = 0.98 $\varepsilon(b_{Gr})$ = 7.35	Gr-Gr = 3.27 BP-Gr = 3.40	-642.01	-112.37
	Gr	$\varepsilon(a_{BP})$ = -0.97 $\varepsilon(a_{BP})$ = -6.84	Gr-Gr = 3.19 BP-Gr = 3.36	-642.38	-129.46
blP/2Gr AA	blP	$\varepsilon(a_{Gr})$ = 0.54	Gr-Gr = 3.46 Gr-blP = 3.36	-792.72	-134.72
	Gr	$\varepsilon(a_{blP})$ = -0.53	Gr-Gr = 3.46 Gr-blP = 3.34	-792.73	-137.22
blP/2Gr AB	blP	$\varepsilon(a_{Gr})$ = 0.54	Gr-Gr = 3.23 Gr-blP =3.43	-792.74	-154.61
	Gr	$\varepsilon(a_{blP})$ = -0.53	Gr-Gr = 3.21 Gr-blP = 3.40	-792.75	-157.67
GP/2Gr AA	GP	$\varepsilon(a_{Gr})$ = 0.76 $\varepsilon(b_{Gr})$ = 10.57	Gr-Gr = 3.53 GP-Gr = 3.30	-641.64	-89.44
	Gr	$\varepsilon(a_{GP})$ = -0.75 $\varepsilon(b_{GP})$ = -9.56	Gr-Gr = 3.30 GP-Gr = 3.25	-641.73	-90.04
GP/2Gr AB	GP	$\varepsilon(a_{Gr})$ = 0.76 $\varepsilon(b_{Gr})$ = 10.57	Gr-Gr = 3.30 GP-Gr = 3.37	-641.65	-98.04
	Gr	$\varepsilon(a_{GP})$ = -0.75 $\varepsilon(b_{GP})$ = -9.56	Gr-Gr = 3.22 GP-Gr = 3.30	-641.74	-100.46

In order to have clear observation on bilayer graphene band structure in the vicinity of the Fermi level, lattice vectors of graphene are adopted in phosphorene/bilayer graphene heterostructures. Figure 8 presents the bandstructures and DOS of black phosphorene/bilayer graphene heterostructures. As in the case of monolayer graphene both black phosphorene and graphene

band structures have been preserved. However, some features have been observed near the Fermi level due to the charge transfer. In the case of AA-stacked bilayer graphene, the graphene Dirac cone is opened by 34.8 meV. The opening of the Dirac cone is related to the charge transfer between phosphorene and bilayer graphene. As indicated in Table.5, the Top (T) layer that interacts directly with phosphorene is differently charged with respect to the bottom (B) layer, which breaks the symmetry between the two graphene planes (top and bottom layers) and opens a gap in the bilayer structure. In the case of AB-stacked bilayer graphene, a Fermi level shift has been observed representing an n-doping in graphene, in addition to the opening of a very small bandgap. As in the case of AA-bilayer graphene, the opening of the Dirac cone is related to symmetry breaking between the two graphene layers due to the difference in charge transfer from black phosphorene to the two graphene layers as indicated in Table.5, which is consistent with various reported studies on bilayer graphene-based interfaces [45−47]. Better illustration of this behavior is presented in Figure 11(a) and Figure 12(a), where the charge distribution shows charge accumulation and depletion only near the top layer of the bilayer graphene (layer in contact with black phosphorene). In that respect, one can obviously notice the charge difference between top and bottom layers in bilayer graphene.

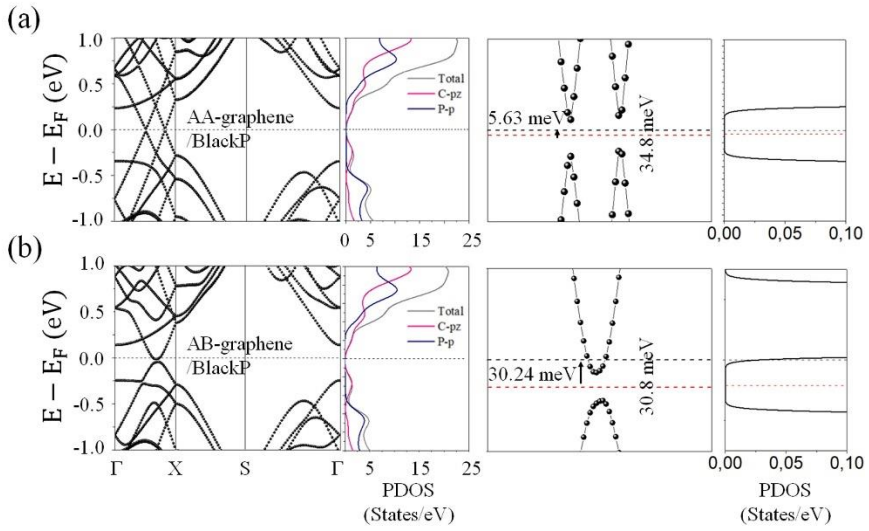

Figure 8 Calculated bandstructures and DOS of (a) black phosphorene/AA-graphene (right), (b) and black phosphorene/AB-graphene. Right panels show the zoom-in band structure near Fermi level. Black and red dashed lines present Fermi level and mid-gap respectively.

Figure 8 presents the bandstructures and DOS of blue phosphorene/bilayer graphene heterostructures. As observed in the case of blue phosphorene/monolayer graphene, blue phosphorene preserves its band structure at the interface with graphene, with a Fermi level shift indicating a p-doping in the bilayer graphene. A higher charge transfer is observed in the case of AA-stacked bilayer graphene, which is in contrast with the black phosphorene/bilayer graphene heterostructure, where AB-stacked bilayer graphene encounters larger charge transfer than AA-stacked bilayer graphene. As mentioned for black phosphorene/bilayer graphene heterostructures, the charge difference between top and bottom layers of the bilayer graphene at the interface with blue phosphorene for AA and AB stacking modes yields a symmetry breaking, resulting in a very small bandgap opening of 10 meV and 11.24 meV respectively.

Indeed, as presented in Figure 11(b) and Figure 12(b), the charge distribution shows a charge transfer only between the top layer of bilayer graphene and blue phosphorene.

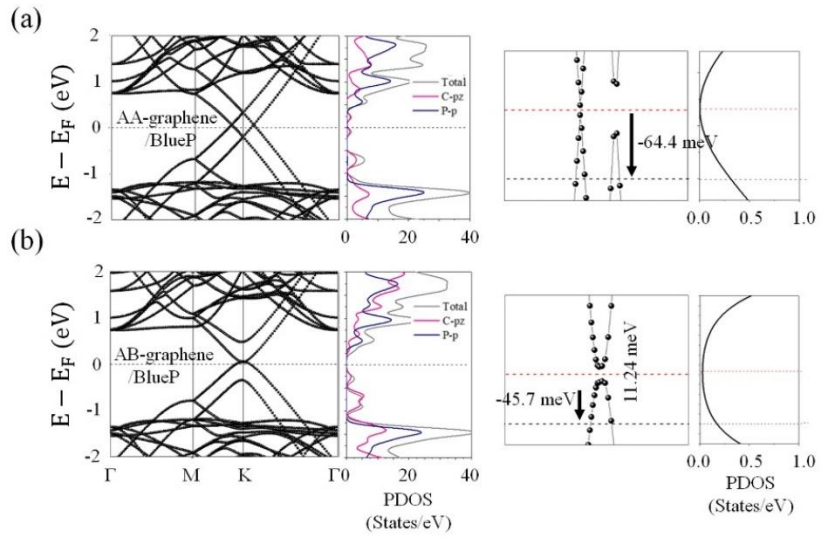

Figure 9 Calculated bandstructures and DOS of (a) blue phosphorene/AA-graphene (right), (b) and blue phosphorene/AB-graphene. Right panels show the zoom-in band structure near Fermi level. Black and red dashed lines present Fermi level and mid-gap respectively.

Finally, in the case of green phosphorene/bilayer graphene heterostructures, we use the green phosphorene lattice vectors, similarly to the monolayer case. Also, both green phosphorene and bilayer graphene electronic bandstructures are preserved. According to Bader charge analysis (Table 5), green phosphorene/bilayer graphene heterostructure exhibits a smaller charge transfer compared to that in black phosphorene and blue phosphorene/bilayer graphene heterostructures. This yields a smaller Fermi level shift, indicating an n-doping in graphene bilayer in both AA- and AB stacking, with a more important charge transfer from green phosphorene to AB-stacked bilayer graphene than to AA-stacked bilayer graphene. According to the results presented in Figure 11(c) (Figure 12(c)), as in the case of green phosphorene/monolayer graphene, the charge distribution in green phosphorene/AA-graphene (green phosphorene/AB-graphene) is much smaller compared to the charge density in black phosphorene and blue phosphorene/bilayer graphene.

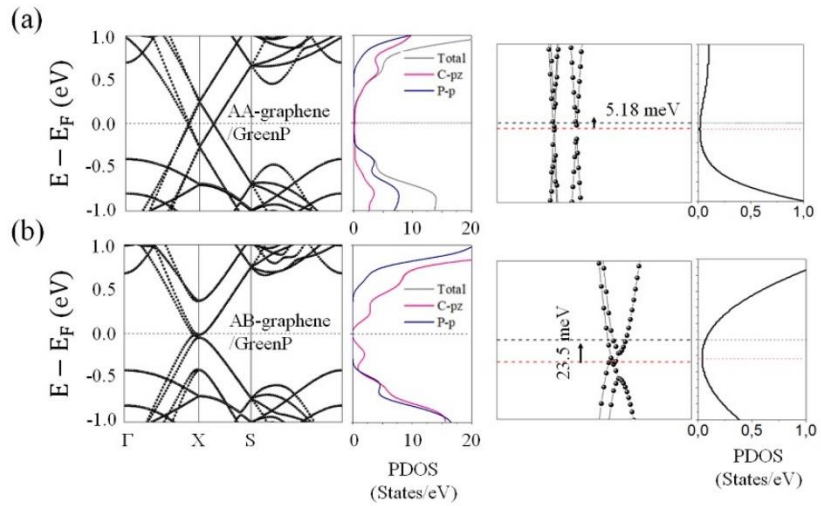

Figure 10 Calculated bandstructures and DOS of (a) green phosphorene/AA-graphene (right), (b) and green phosphorene/AB-graphene. Right panels show the zoom-in band structure near Fermi level. Black and red dashed lines present Fermi level and mid-gap respectively.

Table.5 Calculated Bader charge transfer for phosphorene/bilayer graphene heterostructures. Gr(B) and Gr(T) stand for Bottom and Top layer of bilayer graphene respectively.

	Lattice vectors	Charge Transfer (e^-) (phosphorene to graphene)
BP/2Gr AA	Gr	+0.03; Gr(B) = ~0.00; Gr(T) = +0.03
BP/2Gr AB	Gr	+0.04; Gr(B) = ~0.00; Gr(T) = +0.04
blP/2Gr AA	Gr	-0.05; Gr(B) = ~0.00; Gr(T)= -0.05
blP/2Gr AB	Gr	-0.04; Gr(B) = ~0.00; Gr(T) = -0.04
GP/2Gr AA	GP	+0.01; Gr(B) = ~0.00; Gr(T)= +0.01
GP/2Gr AB	GP	+0.02; Gr(B) = ~0.00; Gr(T)= +0.02

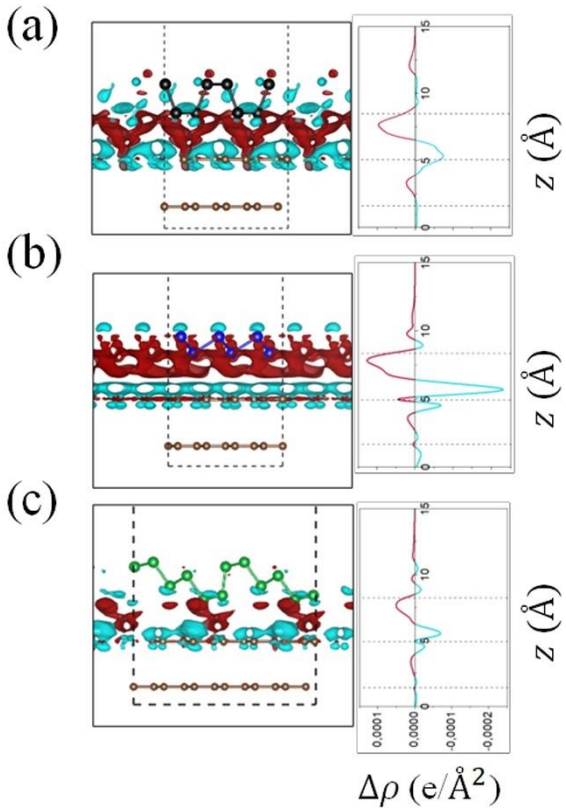

Figure 11 Difference in charge distribution and planar averaged charge density along z-axis in BP/AA-Gr (a), blP/AA-Gr (b), and BP/AA-Gr (c) heterostructures. The cyan and red regions represent charge depletion and accumulation, respectively. The isosurface value is 0.0001 e/Å^3, and horizontal dashed-dot lines denote the locations of atomic layers of graphene and phosphorene.

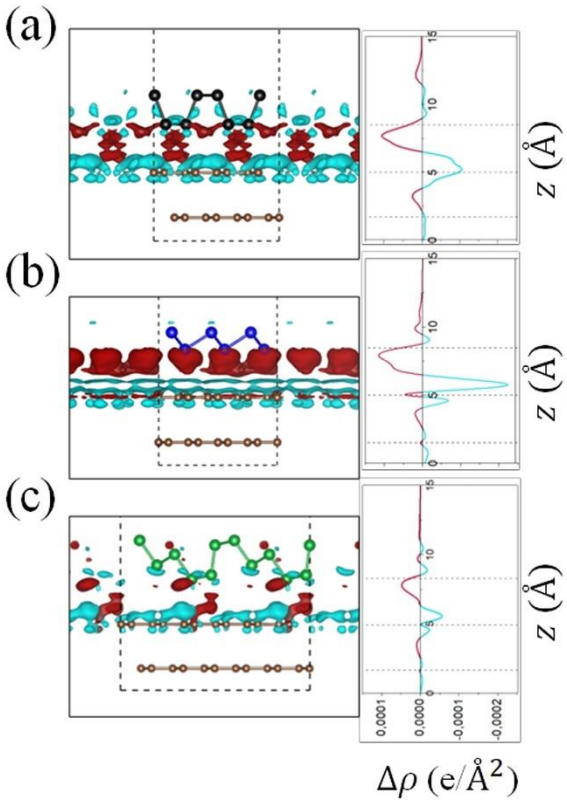

Figure 12 Difference in charge distribution and planar averaged charge density along z-axis in BP/AB-Gr (a), blP/AB-Gr (b), and BP/AB-Gr (c) heterostructures. The cyan and red regions represent charge depletion and accumulation, respectively. The isosurface value is 0.0001 e/Å^3, and horizontal dashed-dot lines denote the locations of atomic layers of graphene and phosphorene.

Conclusion

In summary, a comparative study of black, blue, green phosphorene/graphene is presented. For all the configurations of phosphorene/monolayer graphene, no gap opening near the graphene Dirac cone has been observed. Blue phosphorene/graphene heterostructure presents the lowest interaction energy, and highest charge transfer from graphene to blue phosphorene. Black phosphorene/graphene heterostructure exhibits a higher interaction energy, and a lower charge transfer from black phosphorene to graphene, whereas green phosphorene/graphene heterostructure presents the highest interaction energy. Stability and interaction energies in phosphorene/bilayer graphene heterostructures follow the same trend as in phosphorene/monolayer graphene. Also, a more important charge transfer has been obtained from phosphorene to AB-stacked bilayer graphene than to AA-stacked bilayer graphene for black and green phosphorene. A more important charge transfer is observed from AA-stacked bilayer to blue phosphorene than from AB-stacked bilayer graphene. These charge transfers lead to small gap opening in the bilayer graphene bandstructures due to the charge difference between the top and bottom layers. These results show that different phosphorene allotropes allow modulating graphene or bilayer graphene electronic properties, leading to promising perspectives for future nanoelectronics devices.

Acknowledgment

The research leading to these results has received funding from OCP grant AS70 "Towards phosphorene-based materials and devices".

Computational resources for this study were provided by the computing facilities of High Performance Computing simlab-cluster, of Mohammed VI Polytechnic University at Benguerir.

References

[1] S. C. Dhanabalan, J. S. Ponraj, H. Zhang, Q. Bao. Present perspectives of broadband photodetectors based on nanobelts, nanoribbons, nanosheets and the emerging 2D materials. *Nanoscale*, 2016, *8*(12), 6410-6434.

[2] J. He, L. Tao, H. Zhang, B. Zhou, J. Li. Emerging 2D materials beyond graphene for ultrashort pulse generation in fiber lasers. *Nanoscale*, 2019, *11*(6), 2577-2593.

[3] Y. Wang, M. Qiu, M. Won, E. Jung, T. Fan, N. Xie, & J. S. Kim. Emerging 2D material-based nanocarrier for cancer therapy beyond graphene. *Coord. Chem. Rev* , 2019, *400*, 213041.

[4] Z. Xie, Y. P. Peng, L. Yu, C. Xing, M. Qiu, J. Hu, H. Zhang. Solar-Inspired Water Purification Based on Emerging 2D Materials: Status and Challenges. *Sol. RRL* , 2020, *4*(3), 1900400.

[5] A. S. Bati, M. Batmunkh, J. G. Shapter. Emerging 2D layered materials for perovskite solar cells. *Adv. Energy Mater*., 2020, *10*(13), 1902253.

[6] N. R. Glavin, R. Rao, V. Varshney, E. Bianco, A. Apte, A. Roy, & P. M. Ajayan. Emerging applications of elemental 2D materials. *Adv. Mater*. , 2020, *32*(7), 1904302.

[7] A. Qadir, T. K. Le, M. Malik, K. A. A. Min-Dianey, I. Saeed, Y. Yu, & P. V. Pham. Representative 2D-material-based nanocomposites and their emerging applications: a review. *RSC Adv.* , 2021, *11*(39), 23860-23880.

[8] M. Shrivastava, V. Ramgopal Rao. A Roadmap for Disruptive Applications and Heterogeneous Integration Using Two-Dimensional Materials: State-of-the-Art and Technological Challenges. *Nano Lett.* , 2021, *21*(15), 6359-6381.

[9] M. K. Man, S. Deckoff-Jones, A. Winchester, G. Shi, G. Gupta, A. D. Mohite, K. M. Dani. Protecting the properties of monolayer MoS 2 on silicon based substrates with an atomically thin buffer. *Sci. Rep.* , 2016, *6*(1), 1-9.

[10] X. Han, J. Lin, J. Liu, N. Wang, D. Pan. Effects of hexagonal boron nitride encapsulation on the electronic structure of few-layer MoS2. *J. Phys. Chem. C.* , 2019, *123*(23), 14797-14802.

[11] M. Chhowalla, H. S. Shin, G. Eda, L. J. Li, K. P. Loh, H. Zhang. The chemistry of two-dimensional layered transition metal dichalcogenide nanosheets. *Nat. Chem.* , 2013, *5*(4), 263-275.

[12] W. Choi, N. Choudhary, G. H. Han, J. Park, D. Akinwande, Y. H. Lee. Recent development of two-dimensional transition metal dichalcogenides and their applications. *Mater. Today* , 2017, *20*(3), 116-130.

[13] T. Inoshita, M. Hirayama, N. Hamada, H. Hosono, S. Murakami. Topological semimetal phases manifested in transition metal dichalcogenides intercalated with 3 d metals. *Phys. Rev. B*, 2019, *100*(12), 121112.

[14] M. Samadi, N. Sarikhani, M. Zirak, H. Zhang, H. L. Zhang, A. Z. Moshfegh. Group 6 transition metal dichalcogenide nanomaterials: synthesis, applications and future perspectives. *Nanoscale Horiz.*, 2018. *3*(2), 90-204.

[15] W. Choi, J. Kim, E. Lee, G. Mehta, V. Prasad. Asymmetric 2D MoS2 for Scalable and High-Performance Piezoelectric Sensors. *ACS Appl. Mater. Interfaces*, 2021, *13*(11), 13596-13603.
[16] M. Velický, P. S. Toth. From two-dimensional materials to their heterostructures: An electrochemist's perspective. *Appl. Mater. Today* , 2017, *8*, 68-103.
[17] H. Liu, A. T. Neal, Z. Zhu, Z. Luo, X. Xu, D. Tománek, P. D. Ye. Phosphorene: an unexplored 2D semiconductor with a high hole mobility. *ACS nano*, 2014, *8*(4), 4033-4041.
[18] F. Xia, H. Wang, Y. Jia. Rediscovering black phosphorus as an anisotropic layered material for optoelectronics and electronics. *Nat. Commun.*, 2014, *5*(1), 1-6.
[19] Z. Zhu, D. Tománek. Semiconducting layered blue phosphorus: a computational study. *Phys. Rev. lett.*, 2014, *112*(17), 176802.
[20] W. Zhang, H. Enriquez, Y. Tong, A. Bendounan, A. Kara, A. P. Seitsonen, H. Oughaddou. Epitaxial synthesis of blue phosphorene. *Small*, 2018, *14*(51), 1804066.
[21] W. H. Han, S. Kim, I. H. Lee, K. J. Chang. Prediction of green phosphorus with tunable direct band gap and high mobility. *J. Phys. Chem. Lett.* , 2017, *8*(18), 4627-4632.
[22] A. K. Geim, I. V. Grigorieva. Van der Waals heterostructures. *Nature*, 2013, *499*(7459), 419-425.
[23] M. Yankowitz, Q. Ma, P. Jarillo-Herrero, B. J. LeRoy. Van der Waals heterostructures combining graphene and hexagonal boron nitride. *Nat. Rev. Phys.* , 2019, *1*(2), 112-125.
[24] S. Ghosh, A. Varghese, H. Jawa, Y. Yin, N. V. Medhekar, S. Lodha. Polarity-Tunable Photocurrent through Band Alignment Engineering in a High-Speed WSe2/SnSe2 Diode with Large Negative Responsivity. *ACS Nano*, 2022.
[25] Z. Mansouri et al. Graphene/Phosphorene nano-heterostructure as a potential anode material for (K/Na)-ion batteries: Insights from DFT and AIMD. *Comput. Mater. Sci.*, 2022, 202, 110936.
[26] J. Wang, F. Ma, M. Sun. Graphene, hexagonal boron nitride, and their heterostructures: properties and applications. *RSC adv.*, 2017, *7*(27), 16801-16822.
[27] C. Li, Q. Cao, F. Wang, Y. Xiao, Y. Li, J. J. Delaunay, H. Zhu. Engineering graphene and TMDs based van der Waals heterostructures for photovoltaic and photoelectrochemical solar energy conversion. *Chem. Soc. Rev.*, 2018, *47*(13), 4981-5037.
[28] I. Lee, W. T. Kang, Y. S. Shin, Y. R. Kim, U. Y. Won, K. Kim, W. J. Yu. Ultrahigh gauge factor in graphene/MoS2 heterojunction field effect transistor with variable Schottky barrier. *ACS nano*, 2019, *13*(7), 8392-8400.
[29] G. Iannaccone, F. Bonaccorso, L. Colombo, G. Fiori. Quantum engineering of transistors based on 2D materials heterostructures. *Nat. Nanotechnology*, 2018, *13*(3), 183-191.
[30] H. L. Tang, M. H. Chiu, C. C. Tseng, S. H. Yang, K. J. Hou, S. Y. Wei, L. J. Li. Multilayer graphene–Wse2 heterostructures for WSe2 transistors. *ACS nano*, 2017, *11*(12), 12817-12823.
[31] C. Li, et al. A promising blue phosphorene/C2N van der Waals type-II heterojunction as a solar photocatalyst: a first-principles study. *Phys. Chem. Chem. Phys.*, 2020, 22(2), 615-623.
[32] P. Giannozzi, S. Baroni, N. Bonini, M. Calandra, R. Car, C. Cavazzoni, D. Ceresoli, G. L. Chiarotti, M. Cococcioni, I. Dabo, A. Dal Corso. QUANTUM ESPRESSO: a modular and open-source software project for quantum simulations of materials. *J. Phys. Condens. Matter.*, 2009, 21(39), 395502

[33] J. P. Perdew, K. Burke, M. Ernzerhof. Generalized gradient approximation made simple. *Phys Rev Lett.*, 1996, 77(18), 3865
[34] S. Grimme. Semiempirical GGA-type density functional constructed with a long-range dispersion correction. *J. Comput. Chem.*, 2006, 27(15), 1787–1799.
[35] J. Heyd, G. E. Scuseria, and M. Ernzerhof. Hybrid functionals based on a screened Coulomb potential. *J. Chem. Phys.*, 2003, 118(18), 8207–8215.
[36] J. Heyd, G. E. Scuseria. Efficient hybrid density functional calculations in solids: Assessment of the Heyd–Scuseria–Ernzerhof screened Coulomb hybrid functional. *J. Chem. Phys.* , 2004, *121*(3), 1187-1192.
[37] G. Henkelman, A. Arnaldsson, H. Jonsson. A fast and robust algorithm for Bader decomposition of charge density, *Comput. Mater. Sci.* 2006, 30 (3), 354–360, 36.
[38] D. Shiri, A. Verma, C. R. Selvakumar, M. P. Anantram. Reversible modulation of spontaneous emission by strain in silicon nanowires. *Sci. Rep.*, 2012, *2*(1), 1-10.
[39] J. Noborisaka, K. Nishiguchi, A. Fujiwara. Electric tuning of direct-indirect optical transitions in silicon. *Sci. Rep.*, 2014, *4*(1), 1-6.
[40] Z. Zhu, D. Tománek. Semiconducting layered blue phosphorus: a computational study. *Phys. Rev. lett.*, 2014, *112*(17), 176802.
[41] E. Garrison, C. K. Chan, X. Peng. Size and strain effects on mechanical and electronic properties of green phosphorene nanoribbons. *AIP Adv.*, 2018, *8*(11), 115124.
[42] D. Di Felice, E. Abad, C. González, A. Smogunov, Y. J. Dappe. Angle dependence of the local electronic properties of the graphene/MoS2 interface determined by ab initio calculations. *J. Phys. D: Appl. Phys*, 2017, *50*(17), 17LT02.
[43] Y. Liu, et al. Tailoring sample-wide pseudo-magnetic fields on a graphene–black phosphorus heterostructure. *Nat. Nanotechnol.*, 2018, 13(9), 828-834.
[44] E. Mostaani, N. D. Drummond and V. I. Fal'ko. Quantum Monte Carlo Calculation of the Binding Energy of Bilayer Graphene. *Phys. Rev. Lett.* 2015, 115 (11), 115501
[45] D. Pierucci, H. Sediri, M. Hajlaoui, E. Velez-Fort, Y. J. Dappe, M. G. Silly, A. Ouerghi. Self-organized metal-semiconductor epitaxial graphene layer on off-axis 4H-SiC (0001). *Nano Res.*, 2015, *8*(3), 1026-1037.
[46] M. T. Dau, et al. Beyond van der Waals interaction: the case of MoSe2 epitaxially grown on few-layer graphene. *ACS nano*, 2018, *12*(3), 2319-2331.
[47] Y. J. Dappe, et al. Charge transfers and charged defects in WSe2/graphene-SiC interfaces. *Nanotechnology*, 2020, *31*(25), 255709.